

# Design and Experiment of an Axial-Axial Flux Compound-Structure PMSM Used for HEVs

Jing Zhao, Ping Zheng, *Senior Member, IEEE*, Chengde Tong, Ranran Liu, and Qian Wu

Department of Electrical Engineering, Harbin Institute of Technology, Harbin, China  
zhaojingsnow@gmail.com; zhengping@hit.edu.cn

**Abstract**—An axial-axial flux compound-structure permanent-magnet synchronous machine (CS-PMSM), which is a hybrid electric vehicle (HEV) power train concept, is a structural integration of two axial flux permanent-magnet synchronous machines. It is a novel electromagnetic device with dual mechanical ports and dual electric ports. In this paper, several candidate electromagnetic schemes for the CS-PMSM are analyzed and compared with 3D finite-element method (FEM), and an optimum tradeoff choice for the prototype machine is established. The axial magnetic force, which is unilateral and very important for the assembly, operation and choice of bearings, is evaluated using 3D FEM. A downsized prototype machine of the CS-PMSM was manufactured. The experiments were performed. The magnetic and mechanical designs are evaluated by experimental results.

**Keywords**—Axial-axial flux; compound-structure permanent-magnet synchronous machine; electromagnetic scheme; soft magnetic composite (SMC).

## I. INTRODUCTION

Since the Toyota Prius was marketed in 1997, the electronic continuously variable transmission (e-CVT) propulsion for full hybrids has attracted great interest for automakers and researchers. The Toyota Hybrid System (THS) is composed of a planetary gear, a generator, and a motor. Due to the inevitable mechanical transmission loss, gear noise, and regular lubrication of the planetary gear [1], a new breed of electromagnetic transmission was put forward [2-4], aiming to get rid of mechanical planetary gear while retaining e-CVT function. The electromagnetic transmission integrates of two electric machines, which can be chosen as permanent-magnet synchronous machines, induction machines, or reluctance machines. Different choices lead to different electromagnetic designs and control strategies.

An axial-axial flux compound-structure permanent-magnet synchronous machine (CS-PMSM) is this kind of transmission of permanent-magnet type. The schematic diagram of the axial-axial flux CS-PMSM system is shown in Fig. 1. As the key part of the system, the CS-PMSM is inserted between the internal combustion engine (ICE) and the final gear. It comprises three parts: the stator with three-phase windings, the magnet rotor with permanent magnets (PMs) on both sides, and the winding rotor with three-phase windings fed via slip rings. The stator and magnet rotor operate as one machine called stator machine (SM), and the magnet rotor and winding rotor operate as

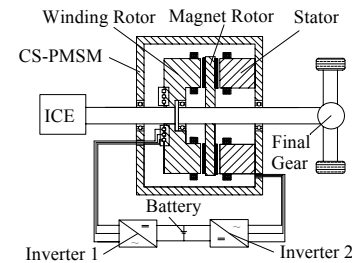


Fig. 1. Schematic diagram of CS-PMSM system.

another machine called double-rotor machine (DRM). The SM and DRM can operate as motor or generator. However, the DRM mainly operate as generator to charge the battery or provide electric power to the SM directly; simultaneously, the DRM transfers the torque of the ICE to the load and offers the speed difference between the ICE and the Load. The SM provides the torque difference between the ICE and the Load. Thus, the CS-PMSM can operate like a continuous variable transmission and keep the ICE operate at high efficiency region.

To validate the concept, the magnetic characteristics, design, manufacture and experiment of a downsized axial-axial flux CS-PMSM with rated power of 20 kW are researched in this paper. The specifications of the SM and DRM are the same: rated power is 10 kW, and base speed is 3000 rpm.

## II. RESEARCH ON ELECTROMAGNETIC SCHEMES

### A. Candidates of Electromagnetic Schemes

As is known, the axial flux machine has 3D flux distributions. To meet the 3D flux characteristics of the axial-axial flux CS-PMSM, different electromagnetic schemes, e.g., stator cores (or winding rotor core, which operates as the “stator” of DRM) with rolled lamination, stator cores with lamination teeth module and stator cores with soft magnetic composite (SMC), are investigated. The stator core with rolled lamination can be made with long sheet of steel rolled up and slots cut during the rolling. For the stator core with lamination teeth module, the teeth are stacked by laminations in radial direction and yoke in axial direction [6]. Then the teeth are inserted into the yoke, as shown in Fig.2. In this case, the shape of the inserted teeth can be rectangle or trapezoid. The rectangle tooth is simpler to be manufactured than the trapezoid teeth, but it cannot utilize space sufficiently. The stator core with SMC is made from powder iron material and can be molded to theoretically any

shape required using a similar process to injection molding of plastics.

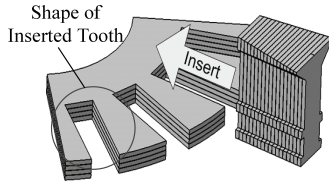


Fig.2 Scheme of lamination teeth module.

### B. Performance of Different Electromagnetic Schemes

As shown in Fig.1, the magnet rotor is a structural and magnetic common part of the SM and DRM. So the magnetic fields of the SM and DRM are coupled in the magnet rotor. The magnetic coupling problem is discussed in Ref. [5], and the result shows that the magnetic decoupling is easy to perform if same pole number and consistent magnetization are adopted for PMs on both sides. So the magnetic performances of the SM and DRM can be investigated separately without considering the magnetic coupling between them. In this section, the performance of one machine, e.g. SM, is researched.

In order to compare the performances of different electromagnetic schemes, the 10-pole 12-slot machine with two-layer concentrated winding is designed and evaluated by 3D finite-element method (FEM). Using the SMC, the back iron core and tooth top can be extended over the end windings to utilize space sufficiently [7]-[8]. The finite element models of different electromagnetic schemes are shown in Figs. 3-5, which are machine of rolled lamination, machine of rectangle and trapezoidal lamination teeth modules, and machine of SMC without and with end extrusion. The performances of machines with different electromagnetic schemes are shown in Table I.

From table I, it can be seen that:

- (1) The machine of rectangle lamination teeth modules has the lowest no-load back EMF and average torque due to its poor space utilization.
- (2) The machine of SMC with end extrusion is very attractive for its no-load back EMF and average torque are much higher than the others.
- (3) Comparing the other three schemes, i.e. rolled lamination, trapezoidal lamination teeth module and SMC without end extrusion, which have almost the same active iron core, It is found that the machine of trapezoidal lamination teeth module has higher back EMF and average torque than the machine with rolled lamination. The machine with SMC without end extrusion has the highest back EMF but lowest average torque among the three schemes, which is different from the usual law of machine. The reason of this result is investigated by analyzing the magnetic characteristics of the three schemes in the following Part C.

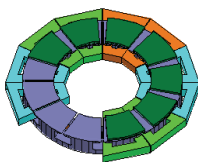


Fig.3 Machine of rolled lamination

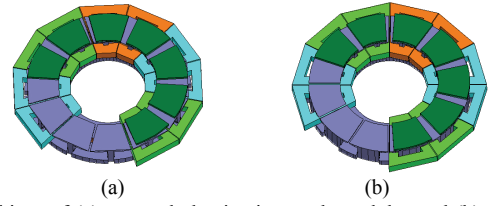


Fig.4 Machines of (a) rectangle lamination teeth modules and (b) trapezoidal lamination teeth modules

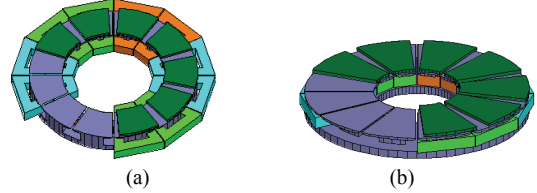


Fig.5 Machines of SMC (a) without end extrusion and (b) with end extrusion

TABLE I  
PERFORMANCE OF DIFFERENT ELECTROMAGNETIC SCHEMES

Electromagnetic Scheme	No-load Back EMF RMS (V)	Average Torque (Nm)
Rolled lamination	88.2435	33.27499
Rectangle lamination teeth modules	67.7034	22.78724
Trapezoidal lamination teeth modules	92.6343	34.06452
SMC without end extrusion	96.9144	30.66441
SMC with end extrusion	129.5233	40.93747

### C. Magnetic Characteristic Analysis

The flux density waveforms in the teeth and yoke along circumferential direction are similar at different radii; and the only difference is the amplitudes at different radii. So, the flux density in teeth and yoke along radial length are analyzed. The inner and outer radii of the air gap of the three schemes, i.e. rolled lamination, trapezoidal lamination teeth module and SMC without end extrusion, are 75mm and 123mm, respectively. Figs. 6 and 7 are the flux density in different parts of the machine along radial length at no-load and load.

As can be seen from Figs.6 and 7 that the distributions in the teeth and yoke of the three schemes are quite different: the flux density amplitude in the teeth decreases with the radius increasing; the flux density amplitude in the yoke increases with the radius increasing; and the change for the scheme of SMC is much less than that of the two other schemes. When laminations are used, the flux is effectively constrained to flow in the 2D surface of the sheet, while the SMC material has 3D isotropic magnetic property, both resulting in the different magnetic properties in different electromagnetic schemes.

As for the flux in the yoke of machine with trapezoidal lamination teeth module from the radius of 60mm to 75mm, it is caused by the protrusion, as shown in Fig.8. And due to the protrusion and the flexible flux path of the yoke, the machine with trapezoidal lamination teeth module has higher back EMF and average torque than the machine with rolled lamination.

The flux density in the teeth and yoke of the machine with SMC without end extrusion is higher at no-load and lower load than the other two schemes, which is in accord with the rule of no-load back EMF and average torque. The explanation is as follows: the SMC material has lower permeability and

saturation flux density than iron lamination material [9], as shown in Fig. 9. But this disadvantage is not obvious and is compensated by the better 3D isotropic magnetic property when the flux density is low at no-load case. However, when the flux density at load is high, this disadvantage is dominant and shows an unsatisfying performance.

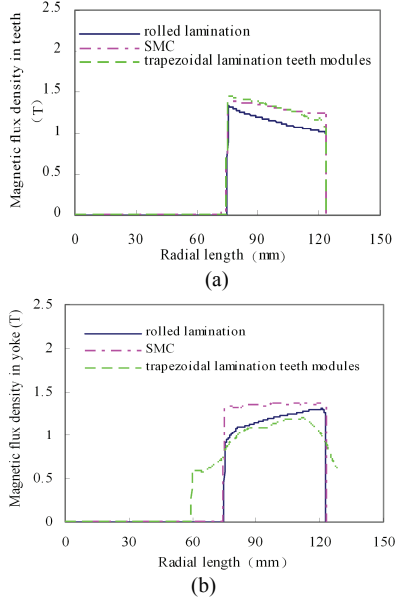


Fig.6 Flux density in (a) teeth and (b) yoke of the machine along radial length at no-load

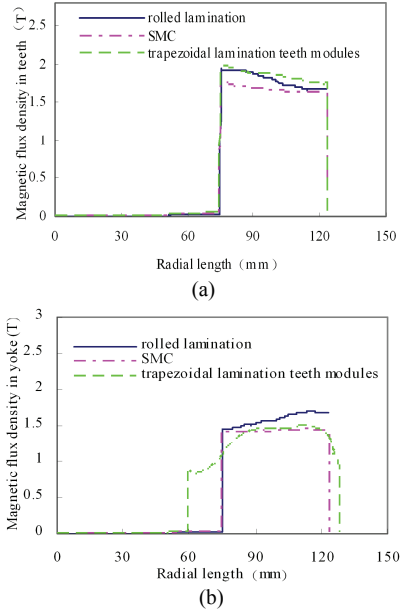


Fig.7 Flux density in (a) teeth and (b) yoke of the machine along radial length at load

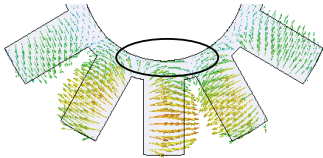


Fig. 8 Flux distribution in the yoke of the machine with trapezoidal lamination teeth module.

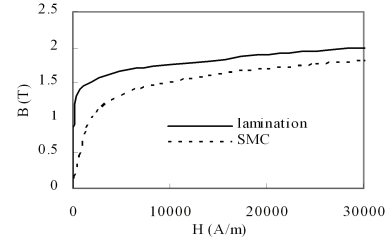


Fig.9 Comparison of the B-H curves of the SMC and lamination.

#### D. Selection of Electromagnetic scheme for Prototype Machine

Summarizing the electromagnetic schemes discussed above, the scheme of SMC with end extrusion is very satisfying and has much potential in the application. But it is not a suitable candidate for a prototype machine considering the manufacture cost for single one machine. The scheme of rolled lamination is more preferred due to its simpler processing technologies than the scheme with trapezoidal lamination teeth module. So a prototype machine with rolled lamination is designed for the testing facilities and concept validation in the following sections.

### III. MECHANICAL DESIGN AND MANUFACTURE OF PROTOTYPE MACHINE

As the axial-axial flux CS-PMSM is a novel machine with dual mechanical ports and dual electric ports, the mechanical structure design is a new attempt in the field of machines.

#### A. Analysis and Calculation of Axial Magnetic Force

As can be seen from Fig. 1, the axial magnetic force on the winding rotor is unilateral, which will be applied on the bearing between the winding rotor and magnet rotor. Similarly, the axial magnetic force between the stator and magnet rotor will be endured by the bearing between them. So, the axial magnetic force is very important for the assembly, operation and choice of bearings [10]. It is calculated with 3D FEM based on the Maxwell's stress tensor method. The axial magnetic force density in the air gap is given by

$$f_a = B_a^2 / 2\mu_0 \quad (1)$$

Then the axial magnetic force is as

$$F_a = \int_0^A \frac{1}{2\mu_0} B_a^2 dS \quad (2)$$

where  $f_a$  is axial magnetic force density,  $B_a$  is the air-gap flux density,  $\mu_0$  is the permeability of free space,  $F_a$  is the axial magnetic force and  $A$  is the area of the air gap. As the magnetic structures of the SM and DRM are the same, the axial magnetic force between the winding rotor and magnet rotor and that between the stator and magnet rotor are the same with both 4973N at no-load.

#### B. Mechanical Structure Design

The mechanical support of the prototype machine is provided by four bearings, i.e., two deep groove ball bearings and two angular contact ball bearings, which are chosen based on the calculated force load, speed and lifetime. The two angular contact ball bearings are installed between the winding

rotor and magnet rotor, the magnet rotor and stator to bear the great attractive force, as illustrated in Fig. 10.

### C. Manufacture of the Prototype Machine

The iron cores of main magnetic components, including winding rotor, magnet rotor and stator, are made of rolled laminations, as shown in Fig.11. After the assembly, it is found that the magnet rotor inclines, which makes the air gaps of the SM and DRM uneven. The schematic diagram and the picture of the uneven air gap are shown in Fig. 12. According to validation from many aspects, it is found that the uneven air gap is caused by the large attractive force and the angular contact ball bearing's property, i.e., its inner ring can move in the axial direction.

## IV. EXPERIMENTAL RESEARCH

Because of the mechanical imperfections, the tests for the prototype are below the speed of 1000 rpm till now.

### A. Back EMF

The back EMF is one of the most important factors that decide the operating voltage, and the sinusoidal degree of back EMF waveform will influence the machine's efficiency, vibration, and noise. The calculated no-load line back EMFs of SM and DRM are the same for their parameters are the same. The calculated and measured no-load line back EMFs of the DRM and SM at 800rpm are shown in Fig. 13. As can be seen from Fig.14, the calculated and measured back EMF waveforms are in good agreements and they are approximately sinusoidal, which validate a good design of the magnetic structure. The measured magnetic performances of the SM and DRM are almost the same, which meet the design requirement.

In order to evaluate the effect of the uneven air gap on the back EMF, the no-load line back EMF of six continuous electric periods at 800 rpm was measured, which includes a

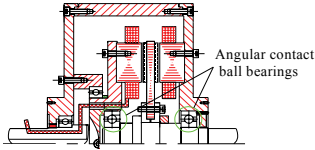
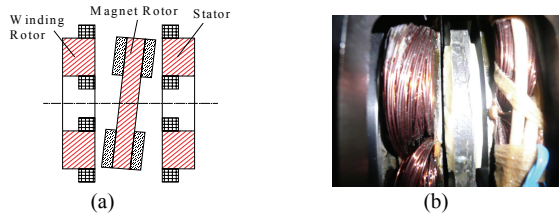


Fig.10 Mechanical structure of the prototype machine.



Fig.11 Main components of the prototype machine.



mechanical period plus an electric period. Fig.14 is the no-load line back EMF waveform of the six continuous electric periods; Table II and Fig.15 are comparisons of no-load line back EMFs of different electric periods and their harmonics, respectively. It can be seen that uneven air gap has little effect on the back EMF; the back EMF of the sixth electric period is basically in

accord with that of the first one, for their mechanical positions and air gap conditions are repeated.

### B. No-load Loss

To evaluate the mechanical structure of the prototype machine, the no-load losses were tested in the generator case. The no-load loss can be separated into iron loss, mechanical loss, and stray loss. It is difficult to measure iron loss and mechanical loss separately in the PM machine, so no-load losses including iron loss and mechanical loss together were measured by a torque/speed sensor at different speeds.

The tests of the DRM were performed by locking the magnet rotor and driving the winding rotor. For the SM tests, the magnet rotor was driven with the winding rotor following at the same speed, which will not produce iron loss in the winding rotor. The no-load losses for the DRM and SM are shown in Fig.16. It can be seen that the no-load losses of the DRM and SM are quite high. From the analytical and FEM calculations, the iron losses of the DRM and SM are no more than 200W at 1000rpm. So it can be deduced that the mechanical loss is very high. Thus, the mechanical structure should be improved to increase the efficiency of the axial-axial flux CS-PMSM, which is very important for the propulsion applications.

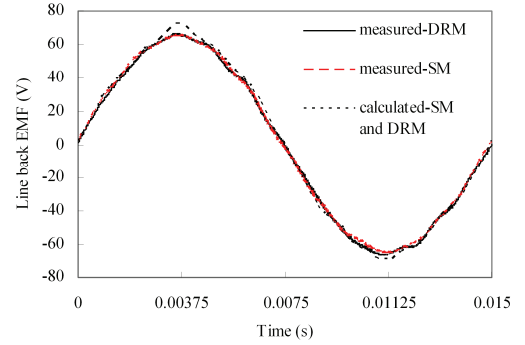


Fig.13 SM and DRM no-load line back EMF.

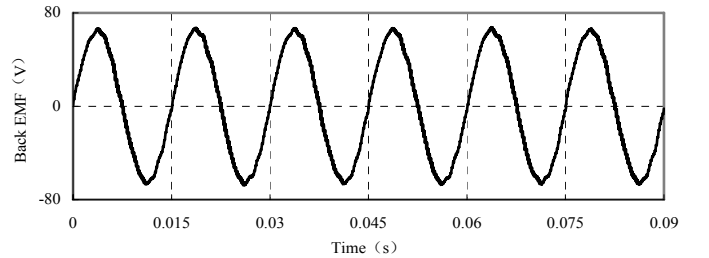


Fig.14 No-load line back EMF of six continuous electric periods.

TABLE II  
COMPARISON OF NO-LOAD LINE BACK EMF

Period No.	Line Back EMF RMS(V)	Changing Rate of Line Back EMF RMS (%)	THD of line Back EMF (%)
6	46.248	0 (reference)	1.98
1	46.2299	-0.03914	1.99
2	45.9905	-0.55678	2.45
3	46.5167	0.580998	1.79
4	45.9145	-0.72111	2.38
5	46.3728	0.26985	1.79

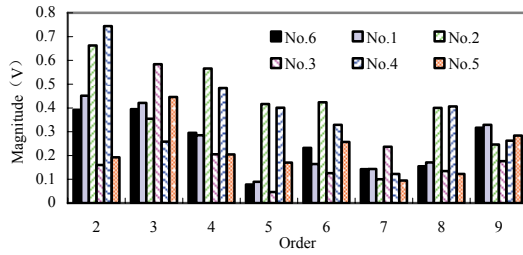


Fig.15 Comparison of back EMF harmonics in different electric periods.

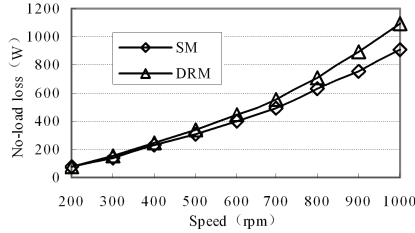


Fig.16 No-load losses for the DRM and SM versus speed.

## V. CONCLUSIONS

An axial-axial flux CS-PMSM, which is integrated by two axial flux PMSMs, is investigated. To meet the 3D flux characteristics of the CS-PMSM, several candidate electromagnetic schemes are analyzed and compared with 3D FEM. Scheme with rolled lamination is selected by tradeoff for the prototype machine. The axial magnetic force is calculated to provide a reference for the mechanical design. A downsized prototype of the CS-PMSM is manufactured. The measured and calculated no-load back EMFs are in good agreement and both validate a good design of the magnetic structure. The no-load losses were tested and analyzed, and the results indicate that the mechanical structure needs to be improved in the future.

## ACKNOWLEDGMENT

This work was supported in part by the 863 Plan of China under Project 2006AA05Z231, in part by National Natural Science Foundation of China under Project 50577011, and in part by Program for New Century Excellent Talents in University under Project NCET-06-0347.

## REFERENCES

- [1] S.M.A. Sharkh, and M.T.N. Mohammad, "Axial Field Permanent Magnet DC Motor With Powder Iron Armature," *IEEE Trans. Energy Convers.*, vol. 22, no. 3, pp. 608–613, 2007.
- [2] P. Curiac, and D. H. Kang, "Preliminary Evaluation of a Megawatt-Class Low-Speed Axial Flux PMSM With Self-Magnetization Function of the Armature Coils," *IEEE Trans. Energy Convers.*, vol. 22, no. 3, pp. 621–628, 2007.
- [3] K. M. Rahman, N. R. Patel, T. G. Ward, J. M. Nagashima, F. Caricchi, and F. Crescimbeni, "Application of Direct-Drive Wheel Motor for Fuel Cell Electric and Hybrid Electric Vehicle Propulsion System," *IEEE Trans. Ind. Appl.*, vol. 42, no. 5, pp. 1185–1192, 2006.
- [4] S. Eriksson, ect, "A four-quadrant HEV drive system," in *Proc. IEEE 56th Vehicular Technology Conf.*, Sep. 2002, vol. 3, pp. 1510–1514.
- [5] P. Zheng, J. Zhao, ect, "Evaluation of the magnetic coupling degree and performance of an axial-axial flux CS-PMSM used for HEVs," *J. Appl. Phys.*, 2008, 103(7): (07F113-1)- (07F113-3).
- [6] Y. D. Chun, ect, "Cogging Torque Reduction in a Novel Axial Flux PM Motor", *International Symposium on Power Electronics, Electrical Drives, Automation and Motion*, 2006, pp. 1020-1023.
- [7] J. Cros, P.Viarouge, A. Halila, "Brush DC Motors with Concentrated Windings and Soft Magnetic Composites Armatures," 2001IEEE, pp. 2549-2556.
- [8] G.S. Liew, E.C.Y. Tsang, ect, "Analysis of a Segmented Brushless PM Machine Utilising Soft Magnetic Composites," *The 33rd Annual Conf. of the IEEE Industrial Electronics Society*, 2007. pp.2268-2273.
- [9] J.B. Wang and D. Howe, "Influence of Soft Magnetic Materials on the Design and Performance of Tubular Permanent Magnet Machines," *IEEE Trans. on Magn.*, 2005, vol.41, no.10, pp. 4057-4059.
- [10] F. Marignetti, ect, "Electromagnetic and Mechanical design of a Fractional-slot-windings Axial-flux PM synchronous machine with Soft Magnetic Compound Stator," *41st IAS Ann. Meeting*, 2006, pp.62-69.